

Probing Gigahertz Coherent Acoustic Phonons in TiO₂ Mesoporous Thin Films

E. R. Cardozo de Oliveira^{*,1}, C. Xiang^{*,1}, M. Esmann^{1,2}, N. Lopez Abdala³, M. C. Fuertes⁴, A. Bruchhausen⁵, H. Pastoriza⁵, B. Perrin⁶, G. J. A. A. Soler-Illia^{**,3}, and N. D. Lanzillotti-Kimura^{**,1}

¹Université Paris-Saclay, CNRS, Centre de Nanosciences et de Nanotechnologies, 91120 Palaiseau, France

²Institute for Physics, University of Oldenburg, 26129 Oldenburg, Germany

³Instituto de NanoSistemas - Universidad Nacional de San Martín-CONICET, Buenos Aires, Argentina

⁴Gerencia Química, Inst. de Nanociencia y Nanotecnología, CNEA-CONICET, Buenos Aires, Argentina

⁵Centro Atómico Bariloche, Inst. de Nanociencia y Nanotecnología, CNEA-CONICET, Rio Negro, Argentina

⁶Sorbonne Université, CNRS, Institut des NanoSciences de Paris, INSP, F-75005 Paris, France

Abstract

Ultrahigh-frequency acoustic-phonon resonators usually require atomically flat interfaces to avoid phonon scattering and dephasing, leading to expensive fabrication processes, such as molecular beam epitaxy. In contrast, mesoporous thin films are based on inexpensive wet chemical fabrication techniques. Here, we report mesoporous titanium dioxide-based acoustic resonators with resonances up to 90 GHz, and quality factors from 3 to 7. Numerical simulations show a good agreement with the picosecond ultrasonics experiments. We also numerically study the effect of changes in the speed of sound on the performance of the resonator. This change could be induced by liquid infiltration into the mesopores. Our findings constitute the first step towards the engineering of building blocks based on mesoporous thin films for reconfigurable optoacoustic sensors.

1 Introduction

Coherent acoustic phonons, with frequencies in the GHz - THz range, have associated wavelengths between a few and hundreds of nanometers. [1, 2, 3, 4, 5, 6, 7, 8, 9] Among other applications, they are suitable for high resolution nanoimaging, non-destructive testing, and sensing. Acoustic phonon dynamics have been explored in systems such as plasmonic nanostructures, [10, 11, 12, 13] metasurfaces, [14] oxides, [15, 16, 17, 18] and semiconductor heterostructures [19, 20, 21, 22] with layer thicknesses on the nanometric scale. [19, 23, 24] To precisely tailor the nanophononic response and obtain high quality devices, expensive and complex growth and processing techniques are usually employed, including molecular beam epitaxy and electron beam lithography.

Conversely, mesoporous structures rely on cheap and reproducible bottom-up fabrication processes derived from soft chemistry, carried out in mild conditions, [25, 26] and are able to sustain gigahertz acoustic resonances. [27, 28, 29] Brillouin light scattering experiments have been employed

*These authors contributed equally to this work

**Corresponding authors: daniel.kimura@c2n.upsaclay.fr, gsoler-illia@unsam.edu.ar

to demonstrate phononic band gaps in the 10 - 20 GHz range in periodic stacks of alternating layers of porous silicon dioxide (SiO_2) and poly-(methyl methacrylate) (PMMA). [27, 30, 31] More recently, mesoporous thin films (MTFs) based on SiO_2 have been shown to support coherent acoustic modes between 5 and 100 GHz, with Q-factors ranging from 5 to 17. [29]. MTFs are also suitable for photonic sensing applications due to the high surface-to-volume ratio and tailorable mesopores. [32, 33] By liquid infiltration into the nanopores, a modulation of the optical and elastic properties of the material could be achieved, also enabling chemical functionalization in nanoacoustic devices. [28, 34]

A well-established material, with numerous applications for both the dense and mesoporous forms, is titanium dioxide (TiO_2). Applications include photocatalysis, [35, 36] implants, [37] photovoltaics, [38] energy harvesting and storage, and sensing. [39] These materials are promising candidates for nanoacoustics. For instance, TiO_2 anatase nanoparticles presented a particularly strong induced exciton shift when applying an acoustic strain pulse. [40, 41]

In this work, we employ coherent phonon generation and detection techniques to study acoustic resonators based on TiO_2 MTFs, with resonances up to 90 GHz. Our results indicate that GHz acoustic resonators based on mesoporous structures are not limited to SiO_2 , and open the possibility to more complex heterostructures formed by different materials. In addition, we theoretically investigate the effect of changes in the elastic properties of the mesoporous matrix on the acoustic resonances, which can be achieved via liquid infiltration into the pores. This platform constitutes a promising building block for developing environment-responsive nanosystems for nanoacoustic sensing and reconfigurable optoacoustic nanodevices based on soft and inexpensive fabrication methods.

2 Experiments and Simulations

2.1 Sample Fabrication

The TiO_2 thin films are synthesized using the sol-gel method. The ordered mesoporosity is obtained using the evaporation-induced self-assembly of surfactants. [25] The fabrication details can be found in reference 29 for silica MTFs, in which the same approach is employed. Ethanolic solutions of TiCl_4 are first prepared, and then the water is added; to obtain the porosity, the surfactant Pluronic F127 is finally added to the precursor solution. The final molar ratio of the sols is $\text{TiCl}_4:\text{H}_2\text{O}:\text{EtOH}$ 1:10:40 to obtain the dense films and $\text{TiCl}_4:\text{F127}:\text{H}_2\text{O}:\text{EtOH}$ 1:0.005:10:40 to synthesize the mesoporous materials. These sols are used immediately after preparation to deposit the films on top of clean Si substrates by dip coating.

The schematics of the studied structure is shown in Fig 1(a). First, a mesostructured titania film is deposited on the substrate and submitted to a stabilization process up to 200°C to consolidate the oxide and stabilize the mesostructure. [44] Then, a capping layer of dense titania is synthesized and stabilized with the same treatment. Afterwards, the bilayer is submitted to a final calcination step of 2 h at 350°C with a $1^\circ\text{C}/\text{min}$ heating ramp; this treatment is performed to eliminate the pores template and generate an accessible and interconnected mesoporosity. [45] Besides, it leads to a phase transition from amorphous titania to anatase. [46] After these steps, homogeneous and crack-free thin films of cm dimensions are achieved.

Afterwards, a ~ 32 nm-thick nickel cover layer is deposited by vacuum thermal evaporation using a homemade system. The dense layer is necessary to avoid nickel diffusion through the mesopores, and the Ni film acts as the acousto-optical transducer for coherent phonon generation and detection. [47]

Four samples are fabricated: three structures designed with different mesoporous layer thicknesses, defined by the dip-coating withdrawal speeds of 1, 2 and 3 mm/s, and one control sample without the mesoporous thin film. The dense layer withdrawal speed is set constant to 0.2 mm/s. The structures are respectively labeled as A, B, C, and Control. Table 1 presents the thickness and porosity parameters, derived from ellipsometry measurements (SOPRA GES5E ellipsometer). [48]

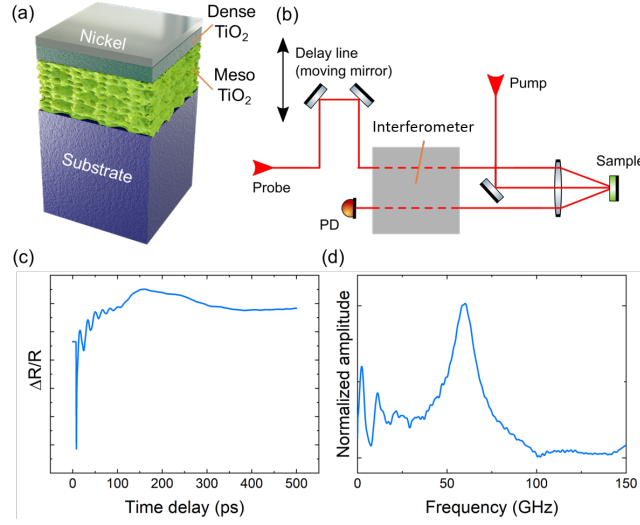


Figure 1: (a) Schematics of the mesoporous TiO_2 sample design. (b) Experimental setup of the reflectometric pump-probe setup. An interferometric measurement can also be implemented, indicated by the gray box. [42, 43] (c) Reflectivity timetrace of the mesoporous TiO_2 sample C. (d) Phononic spectrum corresponding to the timetrace shown in (c).

Table 1: Structural details of the layers from samples A, B, C and Control. Best fit (nominal) thickness values of the dense TiO_2 , nickel and mesoporous layers, and the porosity.

Sample	Mesoporous TiO_2		Dense TiO_2	Ni
	Thickness (nm)	Porosity (%)	Thickness (nm)	
A	110 (103)	48	18 (14)	35 (32)
B	160 (144)	40	30 (26)	31 (32)
C	185 (191)	44	32 (25)	45 (32)
Control	–	–	68 (60)	29.5 (32)

2.2 Coherent phonon generation and detection

The coherent acoustic phonon dynamics is studied via time-domain Brillouin scattering (TDBS) [49] in a pump-probe setup (see Fig. 1(b)). An incident pulsed pump laser ($\lambda = 758$ nm, 200 fs pulse duration, 80 MHz repetition rate, 275 mW equivalent CW power) is partially absorbed by the Ni transducer and excites acoustic phonons via photoinduced stress processes. [49] A second ultrafast laser pulse, namely the probe (typically 5 mW power), delayed with respect to the pump, detects the instantaneous optical reflectivity modulated by the coherent acoustic phonons. Two different processes drive these modulations: the photoelastic interaction, i.e., the changes in the optical properties of the structure due to strain; and the surface displacement induced by the presence of phonons. For the first process, the coherent acoustic phonons induce a change in the index of refraction in the structure proportional to the strain, which will then modulate the reflectivity of the probe. For the latter process, surface displacement detection is performed by implementing a Sagnac interferometer. [42, 43] Further experimental details can be found in Ref. 29. The reflectivity setup is simpler in terms of optical alignment. However, depending on the studied materials and layer ordering, the modulation of the photoelastic properties is weak and the detection of coherent acoustic phonons becomes impossible. In such cases, the interferometric setup must be employed. [42]

Figure 1(c) depicts a typical transient reflectivity timetrace in the interferometric configuration for a TiO₂-based mesoporous sample. Coherent oscillations are visible for time delay < 120 ps. They result from longitudinal coherent phonons modulating the optical properties of the structure. By performing a Fourier transform, we extract the phononic response in the frequency domain (Fig 1(d)).

2.3 Numerical Simulation

To investigate the acoustic resonances, we simulate the acoustic strain, displacement, and electric fields by implementing a transfer matrix method to solve the respective wave equations for a multilayered structure with contrasting refractive indices and acoustic impedances. [50, 51, 52, 53] By calculating the normalized optical and acoustic solutions we can simulate the phonon generation spectrum by integrating the strain, the electric field square modulus and the photoelastic constant. The phonon detection is then obtained by an overlap integral of the generation spectrum with the photoelastic constant, the strain, and the electric field square. [51, 52, 53] The material parameters used in the simulations are shown in Table 2. The surface displacement is also simulated by taking the product of the solutions of the phonon displacement amplitude at the interface between the air and the last layer of the structure, with the phonon generation spectrum. It is assumed that the optical absorption and coherent phonon generation are entirely limited to the nickel transducer layer.

3 Results and Discussion

3.1 Surface displacement and photoelastic interaction

The experimental surface displacement spectra of the TiO₂-based mesoporous samples A, B and C, and the control sample without mesoporous layer, are presented in Fig 2(a). An intense and broad peak is present between 55 GHz and 90 GHz. This peak is associated to an acoustic resonance in the nickel and dense TiO₂ bilayer. [29] At lower frequencies, low amplitude peaks are resolved, which correspond to coherent acoustic phonons confined in the mesoporous layer. For comparison, the results for the mesoporous SiO₂ sample, reported in reference 29, are also displayed in Fig 2(a,b), where the acoustic modes at the mesoporous layer are better resolved. In contrast, the Control structure, without a mesoporous layer, does not show any resonances below 40 GHz, as expected. The spectrum associated to this sample presents a peak at 84.8 GHz, corresponding to the resonance

Table 2: Optical and elastic properties of the studied materials for the numerical simulation. For the mesoporous TiO₂, the index of refraction is derived from the Bruggemann approximation for a mixture of two dielectric media states [54]: dense TiO₂ matrix and the air (pores), according to the porosity on table 1.

Material	Index of refraction	Speed of sound (m/s)	Density (g/cm ³)
TiO ₂	2.56	6700	2.9
SiO ₂	1.5375	5750	2.2
Air	1.00028	343	1.275E-3
Nickel	2.218+4.893i	4970	8.908
TiO ₂ (mesoporous)	(1.76 – 1.90) [54]	4355	2.9

on metallic and dense layers, with a dip at 81.2 GHz, probably originating from a destructive interference between the surface displacement and Brillouin scattering contributions of the signal.

The simulation of the surface displacements are shown in Fig. 2(b). A good agreement between the experimental data and simulation results is achieved. The interference dip present in the Control sample is not reproduced in the simulation as Brillouin scattering is not considered simultaneously with the surface displacement effect. Furthermore, the experimental results of sample C show a dip at ~ 100 GHz, whereas a peak at the same frequency is present in the simulation.

In order to get a finer picture of the phononic behavior of these structures, it is worth comparing the signals -measured and calculated- corresponding to the surface displacement (interferometry) and modulation of the index of refraction (reflectometry, photoelastic effect). Figures 3(a) and (b) display the phononic spectra of both modulation effects for the TiO₂ (sample B) and SiO₂ structures, respectively. For both materials, the intense peak is present in the two cases. However, the lower frequency confined modes are observed uniquely in the interferometric dataset, in which the first five acoustic resonances at 12.6, 23.9, 36.9, 47.7 and 57.9 GHz have respective quality factors of 2.7, 4.7, 4.1, 3.9 and 6.9, within a 10% error.

Simulations for the surface displacement and the photoelastic interaction for both structures are displayed as red-shadowed lines in Figs. 3(a) and (b). They reproduce the main peaks of the experimental datasets for both cases. Furthermore, the low-frequency modes in the photoelastic interaction calculation, associated to the mesoporous resonances, are negligible when compared to the interferometric simulation, in accordance with the experimental results.

The lack of a photoelastic interaction contribution in both experiment and simulation supports the hypothesis that the respective vibrational resonances are confined in the mesoporous layer. Note that the mesoporous material is transparent for the incident laser wavelength -with an associated weak photoelastic constant-. For the surface displacement results, the acoustic modes in the soft mesoporous layer leads the whole structure to vibrate, thus, contributing to the interferometric detection.

3.2 Surface displacement dependence on TiO₂ speed of sound

Elastic properties of TiO₂ thin films, such as mass density (ρ), Young's modulus (Y) and speed of sound (v) depend on several factors such as fabrication method, layer thickness, annealing temperature and crystallinity. This dependence leads to a broad range of reported values for ρ (from 2.9 to

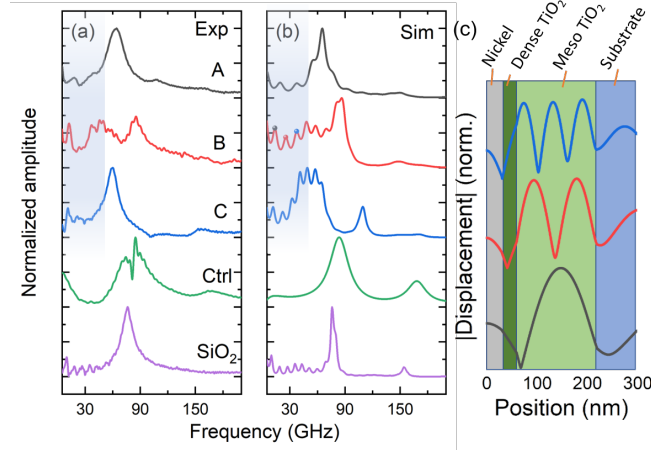


Figure 2: (a) Experimental and (b) simulated spectra of the surface displacement of TiO₂-based samples A, B, C and Control, and SiO₂-based sample C (Ref. 29), for comparison. The low-frequency-shaded areas (up to 50 GHz) indicate the first confined modes in the mesoporous layer. (c) Displacement field of the modes at 13, 25.5 and 38 GHz on TiO₂ sample B, respectively indicated as black, red and blue circles in (b).

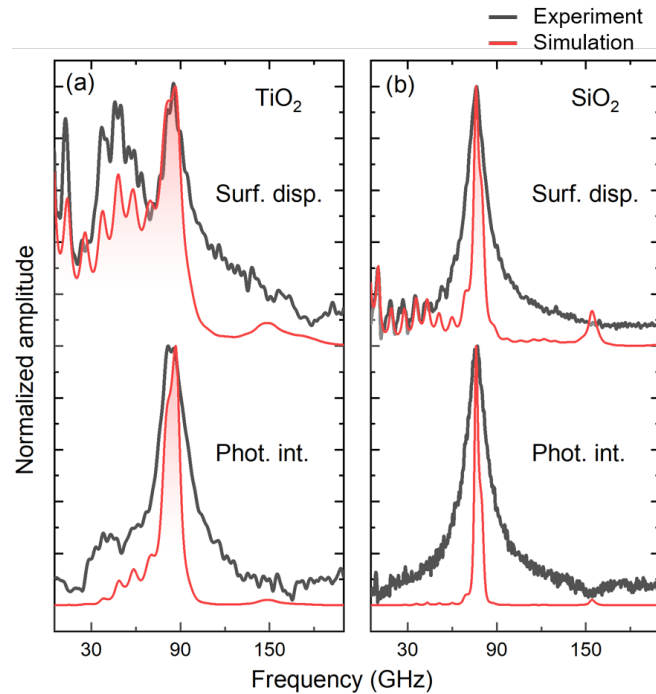


Figure 3: Experimental results (black line) and the respective TMM simulations (red area) on surface displacement and photoelastic interaction for (a) TiO₂ sample B and (b) SiO₂ sample C, from reference 29. Acoustic modes at the low-frequency region are only present at the surface displacement spectra for both TiO₂ and SiO₂.

3.9 g/cm³) and Y (from 80 to 250 GPa), for TiO₂ in its anatase phase. [55, 56, 57, 58, 59, 60, 61, 62] The speed of propagation of longitudinal acoustic modes is calculated according to:

$$v = \sqrt{\frac{Y(1 - \nu)}{\rho(1 + \nu)(1 - 2\nu)}}, \quad (1)$$

where ν is the Poisson ratio. Considering a Poisson ratio of 0.27 for TiO₂, the broad range of values for Y and ρ lead to inaccurate values of longitudinal acoustic waves speed, spanning from 5500 to 11000 m/s. A precise determination of these parameters is out of the scope of this work, however a quantitative analysis is required for the numerical simulations and further discussion.

We simulate the surface displacement at different TiO₂ sound speeds for the control sample, within the range of 6000 to 10000 m/s, and present the results on Fig. 4(a), in a colorplot. The spectrum that best matches with the experiment is simulated with $v_{TiO_2} = 6700$ m/s, indicated by a dashed red line. The density used in the simulation is set constant at 2.9 g/cm³. The TiO₂ dense layer parameters are then used as input for the calculation of the mesoporous samples.

The mesoporous TiO₂ layer parameters are extracted according to the layer porosity and the dense TiO₂ constants. The refractive index is calculated using the Bruggemann approximation of a complex composite by an effective homogeneous medium for a mixture of two dielectric media states. [54] The mass density is considered to be the same as the dense layer, [29] and the speed of sound in the mesoporous material is varied to match with the experimental results. The evolution of the surface displacement spectrum as a function of the ratio between the sound velocities of the mesoporous and dense TiO₂ layers for the three samples is shown on the three panels of Fig. 4(b). The dashed red lines indicate the ratio of the sound velocities for which the simulations best match with the experimental results ($v_{meso} = 4355$ m/s), and the respective spectra are displayed in Fig. 2(b). They exhibit a good agreement with the experiment after adjustments on the layers thicknesses according to the values from Table 1, with a maximum deviation of 11% from the nominal values for the MTFs. We also consider acoustic losses with an effective phonon decay length of ~ 75 nm. [29, 63]. Considering the values $v_{meso} = 4355$ m/s, $\rho = 2.9$ g/cm³ and the Poisson ratio for mesoporous materials $\nu = 0.2$, we deduce that the Young's modulus of the thin films is ~ 49.5 GPa. Although this method of deducing Young's modulus is not standard, the estimated value is in close agreement with the ones reported in the literature, between 37 and 50 GPa. [64, 65]

In Fig. 4(b) we observe a clear increase in mode frequency for the low-frequency modes upon rising the speed of sound in the mesoporous layer. In contrast, the high-frequency modes are hardly affected. This implies that the low-frequency resonances are indeed mainly confined within the MTF. It is worth mentioning that the studied variation of the sound velocity in the mesoporous layer can be experimentally achieved by liquid infiltration into the nanopores, which modifies the elastic properties of the effective medium composed of the TiO₂ dense matrix and air in the pores. As chemical adsorption and capillary condensation are reversible processes, MTFs can be employed as active elements in optoacoustic sensing devices.

The results exhibited in this section are compatible with what has been reported on SiO₂ mesoporous systems, [29] and reinforce the feasibility of coherent acoustic phonon generation and detection in different mesoporous materials. Furthermore, this work reinforces the concept of mesoporous thin films as potential environment-responsive platforms able to transduce a physicochemical process (adsorption, capillary condensation) into optical [26, 32, 33] or nanoacoustic signals [29]. This building block represents an important step towards the engineering of more complex structures based on such soft materials for practical applications, e.g., sensing.

4 Conclusion

In this work we have demonstrated the confinement of gigahertz coherent acoustic phonons in mesoporous titanium dioxide structures, extending the concept of mesoporous acoustic resonators

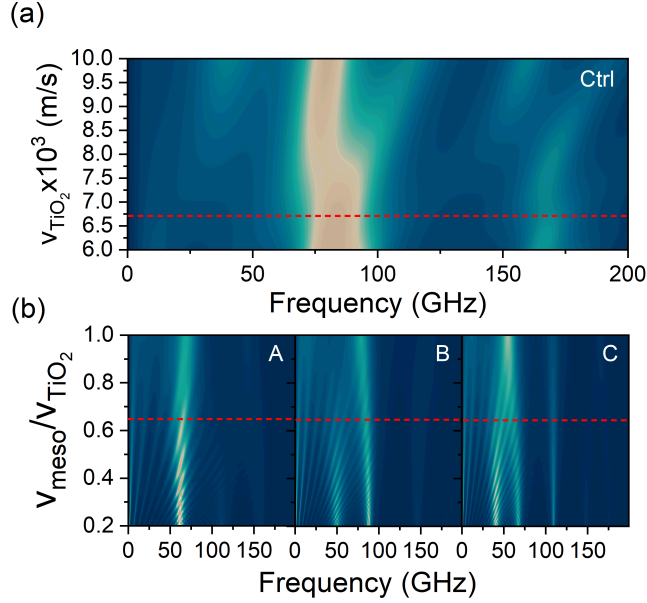


Figure 4: Colorplot of surface displacement amplitude vs frequency and (a) dense TiO_2 speed of sound for control sample, and (b) speed of sound ratio between mesoporous and dense materials for mesoporous TiO_2 -based samples. The dashed lines at $V_{TiO_2} = 6700$ m/s and $V_{meso}/V_{TiO_2} = 0.65$ correspond to the values that best match with experimental results.

to different material systems. Simulations on photoelastic interaction and surface displacement convey appreciable agreement with the experimental results. Furthermore, we discussed the effects of changes in the elastic parameters on the mesoporous resonator performance. These changes can be induced by chemical compound infiltration. This concept can be extended and applied to novel sensing devices based on ultrahigh-frequency resonators, with the mesoporous layer as the active optoacoustic element. Our findings unlock the way to a promising platform for nanoacoustic sensing and reconfigurable optoacoustic nanodevices based on soft, inexpensive fabrication methods.

5 Acknowledgment

The authors acknowledge funding by the European Research Council Starting Grant No. 715939, Nanophennec, the ECOS-Sud Program through the project TUNA-Phon (PA19N03), and through a public grant overseen by the ANR as part of the “Investissements d’Avenir” program (Labex NanoSaclay Grant No. ANR-10-LABX-0035). GJAASI acknowledges ANPCyT for projects PICT 2017-4651, PICT-2018-04236 and PICT 2020-03130. MCF acknowledges ANPCyT for projects PICT 2015-0351 and 2017-1133. ME acknowledges funding by the University of Oldenburg through a Carl von Ossietzky Young Researchers’ Fellowship. NDLC and GJAASI acknowledge funding from CNRS through the project IEA RANas.

6 Authors contributions

GJAASI and NDLC proposed the concepts and directed the research. NLA, MCF, AB, HP, and GJAASI fabricated and characterized the samples. BP and NDLC performed the picosecond ultrasonics experiments. ERCO, CX, ME, NLA, and NDLC performed the simulations and analyzed the data.

References

- [1] M. Trigo, A. Bruchhausen, A. Fainstein, B. Jusserand, and V. Thierry-Mieg. Confinement of acoustical vibrations in a semiconductor planar phonon cavity. *Phys. Rev. Lett.*, 89:227402, Nov 2002.
- [2] Alexander A. Balandin. Nanophononics: Phonon Engineering in Nanostructures and Nanodevices. *Journal of Nanoscience and Nanotechnology*, 5(7):1015–1022, July 2005.
- [3] G. Rozas, M. F. Pascual Winter, B. Jusserand, A. Fainstein, B. Perrin, E. Semenova, and A. Lemaître. Lifetime of THz Acoustic Nanocavity Modes. *Physical Review Letters*, 102(1):015502, January 2009.
- [4] R. P. Beardsley, A. V. Akimov, M. Henini, and A. J. Kent. Coherent Terahertz Sound Amplification and Spectral Line Narrowing in a Stark Ladder Superlattice. *Physical Review Letters*, 104(8):085501, February 2010.
- [5] Sebastian Volz, Jose Ordonez-Miranda, Mika Prunnila Andrey Shchepetov, Jouni Ahopelto, Thomas Pezeril, Gwenaelle Vaudel, Vitaly Gusev, Pascal Ruello, Eva M. Weig, Martin Schubert, Mike Hettich, Martin Grossman, Thomas Dekorsy, Francesc Alzina, Bartłomiej Graczykowski, Emigdio Chavez-Angel, J. Sebastian Reparaz, Markus R. Wagner, Clivia M. Sotomayor-Torres, Shiyun Xiong, Sanghamitra Neogi, and Davide Donadio. Nanophononics: State of the art and perspectives. *European Physical Journal B*, 89(1):15, 2016.
- [6] Fabricio Della Picca, Rodrigo Berte, Mohsen Rahmani, Pablo Albella, Juan M. Bujjamer, Martín Poblet, Emiliano Cortés, Stefan A. Maier, and Andrea V. Bragas. Tailored Hypersound Generation in Single Plasmonic Nanoantennas. *Nano Letters*, 16(2):1428–1434, February 2016.
- [7] F. R. Lamberti, Q. Yao, L. Lanco, D. T. Nguyen, M. Esmann, A. Fainstein, P. Sesin, S. Anguiano, V. Villafañe, A. Bruchhausen, P. Senellart, I. Favero, and N. D. Lanzillotti-Kimura. Optomechanical properties of GaAs/AlAs micropillar resonators operating in the 18 GHz range. *Optics Express*, 25(20):24437, October 2017.
- [8] Marta De Luca, Claudia Fasolato, Marcel A. Verheijen, Yizhen Ren, Milo Y. Swinkels, Sebastian Kölling, Erik P. A. M. Bakkers, Riccardo Rurali, Xavier Cartoixa, and Ilaria Zardo. Phonon Engineering in Twinning Superlattice Nanowires. *Nano Letters*, 19(7):4702–4711, July 2019.
- [9] M. Esmann, F. R. Lamberti, A. Harouri, L. Lanco, I. Sagnes, I. Favero, G. Aubin, C. Gomez-Carbonell, A. Lemaître, O. Krebs, P. Senellart, and N. D. Lanzillotti-Kimura. Brillouin scattering in hybrid optophononic Bragg micropillar resonators at 300 GHz. *Optica*, 6(7):854, July 2019.
- [10] A. Arbouet, N. Del Fatti, and F. Vallee. Optical control of the coherent acoustic vibration of metal nanoparticles. *The Journal of Chemical Physics*, 124(14):144701, April 2006.
- [11] Kevin O’Brien, N. D. Lanzillotti-Kimura, Junsuk Rho, Haim Suchowski, Xiaobo Yin, and Xiang Zhang. Ultrafast acousto-plasmonic control and sensing in complex nanostructures. *Nature Communications*, 5(1):4042, September 2014.
- [12] Yannick Guillet, Allaoua Abbas, Serge Ravaine, and Bertrand Audoin. Ultrafast microscopy of the vibrational landscape of a single nanoparticle. *Applied Physics Letters*, 114(9):091904, March 2019.
- [13] Martin Poblet, Rodrigo Berté, Hilario D. Boggiano, Yi Li, Emiliano Cortés, Gustavo Grinblat, Stefan A. Maier, and Andrea V. Bragas. Acoustic Coupling between Plasmonic Nanoantennas: Detection and Directionality of Surface Acoustic Waves. *ACS Photonics*, 8(10):2846–2852, October 2021.

- [14] Norberto D. Lanzillotti-Kimura, Kevin P. O'Brien, Junsuk Rho, Haim Suchowski, Xiaobo Yin, and Xiang Zhang. Polarization-controlled coherent phonon generation in acoustoplasmonic metasurfaces. *Physical Review B*, 97(23):235403, June 2018.
- [15] A. Soukiassian, W. Tian, D. A. Tenne, X. X. Xi, D. G. Schlom, N. D. Lanzillotti-Kimura, A. Bruchhausen, A. Fainstein, H. P. Sun, X. Q. Pan, A. Cros, and A. Cantarero. Acoustic Bragg mirrors and cavities made using piezoelectric oxides. *Applied Physics Letters*, 90(4):042909, January 2007.
- [16] N. D. Lanzillotti-Kimura, A. Fainstein, B. Perrin, B. Jusserand, A. Soukiassian, X. X. Xi, and D. G. Schlom. Enhancement and Inhibition of Coherent Phonon Emission of a Ni Film in a BaTiO₃ / SrTiO₃ Cavity. *Physical Review Letters*, 104(18):187402, May 2010.
- [17] Thomas Vasileiadis, Jeena Varghese, Visnja Babacic, Jordi Gomis-Bresco, Daniel Navarro Urrios, and Bartłomiej Graczykowski. Progress and perspectives on phononic crystals. *Journal of Applied Physics*, 129(16):160901, April 2021.
- [18] Yu Cang, Yabin Jin, Bahram Djafari-Rouhani, and George Fytas. Fundamentals, progress and perspectives on high-frequency phononic crystals. *Journal of Physics D: Applied Physics*, 55(19):193002, May 2022.
- [19] N. D. Lanzillotti-Kimura, A. Fainstein, B. Jusserand, and A. Lemaître. Resonant Raman scattering of nanocavity-confined acoustic phonons. *Physical Review B*, 79(3):035404, January 2009.
- [20] S. Anguiano, A. E. Bruchhausen, B. Jusserand, I. Favero, F. R. Lamberti, L. Lanco, I. Sagnes, A. Lemaître, N. D. Lanzillotti-Kimura, P. Senellart, and A. Fainstein. Micropillar Resonators for Optomechanics in the Extremely High 19–95-GHz Frequency Range. *Physical Review Letters*, 118(26):263901, June 2017.
- [21] D. L. Chafatinos, A. S. Kuznetsov, S. Anguiano, A. E. Bruchhausen, A. A. Reynoso, K. Biermann, P. V. Santos, and A. Fainstein. Polariton-driven phonon laser. *Nature Communications*, 11(1):4552, December 2020.
- [22] O. Ortiz, P. Priya, A. Rodriguez, A. Lemaitre, M. Esmann, and N. D. Lanzillotti-Kimura. Topological optical and phononic interface mode by simultaneous band inversion. *Optica*, 8(5):598, May 2021.
- [23] G. Arregui, O. Ortíz, M. Esmann, C. M. Sotomayor-Torres, C. Gomez-Carbonell, O. Mauguin, B. Perrin, A. Lemaître, P. D. García, and N. D. Lanzillotti-Kimura. Coherent generation and detection of acoustic phonons in topological nanocavities. *APL Photonics*, 4(3):030805, March 2019.
- [24] N. D. Lanzillotti-Kimura, A. Fainstein, B. Perrin, B. Jusserand, L. Largeau, O. Mauguin, and A. Lemaitre. Enhanced optical generation and detection of acoustic nanowaves in microcavities. *Physical Review B*, 83(20):201103, May 2011.
- [25] G. J. A. A. Soler-Illia and P. Innocenzi. Mesoporous Hybrid Thin Films: The Physics and Chemistry Beneath. *Chemistry - A European Journal*, 12(17):4478–4494, June 2006.
- [26] Rodrigo Martínez Gazoni, Martín G. Bellino, M. Cecilia Fuertes, Gustavo Giménez, Galo J. A. A. Soler-Illia, and María Luz Martínez Ricci. Designed nanoparticle–mesoporous multi-layer nanocomposites as tunable plasmonic–photonic architectures for electromagnetic field enhancement. *Journal of Materials Chemistry C*, 5(14):3445–3455, 2017.
- [27] N. Gomopoulos, D. Maschke, C. Y. Koh, E. L. Thomas, W. Tremel, H.-J. Butt, and G. Fytas. One-Dimensional Hypersonic Phononic Crystals. *Nano Letters*, 10(3):980–984, March 2010.

- [28] Giulio Benetti, Marco Gandolfi, Margriet J. Van Bael, Luca Gavioli, Claudio Giannetti, Claudia Caddeo, and Francesco Banfi. Photoacoustic sensing of trapped fluids in nanoporous thin films: Device engineering and sensing scheme. *ACS Applied Materials & Interfaces*, 10(33):27947–27954, 2018. PMID: 30039696.
- [29] Nicolas Lopez Abdala, Martin Esmann, Maria C. Fuertes, Paula C. Angelomé, Omar Ortiz, Axel Bruchhausen, Hernan Pastoriza, Bernard Perrin, Galo J. A. A. Soler-Illia, and Norberto D. Lanzillotti-Kimura. Mesoporous thin films for acoustic devices in the gigahertz range. *The Journal of Physical Chemistry C*, 124(31):17165–17171, 2020.
- [30] Dirk Schneider, Faroha Liaqat, El Houssaine El Boudouti, Youssef El Hassouani, Bahram Djafari-Rouhani, Wolfgang Tremel, Hans-Jürgen Butt, and George Fytas. Engineering the Hypersonic Phononic Band Gap of Hybrid Bragg Stacks. *Nano Letters*, 12(6):3101–3108, June 2012.
- [31] Dirk Schneider, Faroha Liaqat, El Houssaine El Boudouti, Ossama El Abouti, Wolfgang Tremel, Hans-Jürgen Butt, Bahram Djafari-Rouhani, and George Fytas. Defect-Controlled Hypersound Propagation in Hybrid Superlattices. *Physical Review Letters*, 111(16):164301, October 2013.
- [32] Baptiste Auguié, María Cecilia Fuertes, Paula C. Angelomé, Nicolás López Abdala, Galo J. A. A. Soler Illia, and Alejandro Fainstein. Tamm Plasmon Resonance in Mesoporous Multilayers: Toward a Sensing Application. *ACS Photonics*, 1(9):775–780, September 2014.
- [33] M. C. Fuertes, F. J. López-Alcaraz, M. C. Marchi, H. E. Troiani, V. Luca, H. Míguez, and G. J. A. A. Soler-Illia. Photonic Crystals from Ordered Mesoporous Thin-Film Functional Building Blocks. *Advanced Functional Materials*, 17(8):1247–1254, May 2007.
- [34] Marc Thelen, Nicolas Bochud, Manuel Brinker, Claire Prada, and Patrick Huber. Laser-excited elastic guided waves reveal the complex mechanics of nanoporous silicon. *Nature Communications*, 12(1):3597, June 2021.
- [35] S. Suárez, N. Arconada, Y. Castro, J.M. Coronado, R. Portela, A. Durán, and B. Sánchez. Photocatalytic degradation of TCE in dry and wet air conditions with TiO₂ porous thin films. *Applied Catalysis B: Environmental*, 108–109:14–21, October 2011.
- [36] Abdulmenan M. Hussein, Luther Mahoney, Rui Peng, Harrison Kibombo, Chia-Ming Wu, Ranjit T. Koodali, and Rajesh Shende. Mesoporous coupled ZnO/TiO₂ photocatalyst nanocomposites for hydrogen generation. *Journal of Renewable and Sustainable Energy*, 5(3):033118, May 2013.
- [37] N. Harmankaya, J. Karlsson, A. Palmquist, M. Halvarsson, K. Igawa, M. Andersson, and P. Tengvall. Raloxifene and alendronate containing thin mesoporous titanium oxide films improve implant fixation to bone. *Acta Biomaterialia*, 9(6):7064–7073, June 2013.
- [38] Ianina L. Violi, M. Dolores Perez, M. Cecilia Fuertes, and Galo J. A. A. Soler-Illia. Highly Ordered, Accessible and Nanocrystalline Mesoporous TiO₂ Thin Films on Transparent Conductive Substrates. *ACS Applied Materials & Interfaces*, 4(8):4320–4330, August 2012.
- [39] Jia Hong Pan, X.S. Zhao, and Wan In Lee. Block copolymer-templated synthesis of highly organized mesoporous TiO₂-based films and their photoelectrochemical applications. *Chemical Engineering Journal*, 170(2-3):363–380, June 2011.
- [40] Edoardo Baldini, Tania Palmieri, Adriel Dominguez, Pascal Ruello, Angel Rubio, and Majed Chergui. Phonon-Driven Selective Modulation of Exciton Oscillator Strengths in Anatase TiO₂ Nanoparticles. *Nano Letters*, 18(8):5007–5014, August 2018.

- [41] Edoardo Baldini, Adriel Dominguez, Tania Palmieri, Oliviero Cannelli, Angel Rubio, Pascal Ruello, and Majed Chergui. Exciton control in a room temperature bulk semiconductor with coherent strain pulses. *Science Advances*, 5(11):eaax2937, November 2019.
- [42] B Perrin, C Rossignol, B Bonello, and J.-C Jeannet. Interferometric detection in picosecond ultrasonics. *Physica B: Condensed Matter*, 263–264:571–573, March 1999.
- [43] O. Matsuda and O. B. Wright. Reflection and transmission of light in multilayers perturbed by picosecond strain pulse propagation. *Journal of the Optical Society of America B*, 19(12):3028, December 2002.
- [44] P. C. Angelomé, M. C. Fuertes, and G. J. A. A. Soler-Illia. Multifunctional, Multilayer, Multiscale: Integrative Synthesis of Complex Macroporous and Mesoporous Thin Films with Spatial Separation of Porosity and Function. *Advanced Materials*, 18(18):2397–2402, September 2006.
- [45] María Cecilia Fuertes, Silvia Colodrero, Gabriel Lozano, Agustín R. González-Elipe, David Grosso, Cédric Boissière, Clément Sánchez, Galo J. de A. A. Soler-Illia, and Hernán Míguez. Sorption Properties of Mesoporous Multilayer Thin Films. *The Journal of Physical Chemistry C*, 112(9):3157–3163, March 2008.
- [46] Galo J. A. A. Soler-Illia, Paula C. Angelomé, M. Cecilia Fuertes, David Grosso, and Cedric Boissiere. Critical aspects in the production of periodically ordered mesoporous titania thin films. *Nanoscale*, 4(8):2549, 2012.
- [47] A. Huynh, N. D. Lanzillotti-Kimura, B. Jusserand, B. Perrin, A. Fainstein, M. F. Pascual-Winter, E. Peronne, and A. Lemaître. Subterahertz Phonon Dynamics in Acoustic Nanocavities. *Physical Review Letters*, 97(11):115502, September 2006.
- [48] Cédric Boissiere, David Grosso, Sophie Lepoutre, Lionel Nicole, Aline Brunet Bruneau, and Clément Sanchez. Porosity and Mechanical Properties of Mesoporous Thin Films Assessed by Environmental Ellipsometric Porosimetry. *Langmuir*, 21(26):12362–12371, December 2005.
- [49] Pascal Ruello and Vitalyi E. Gusev. Physical mechanisms of coherent acoustic phonons generation by ultrafast laser action. *Ultrasonics*, 56:21–35, February 2015.
- [50] C. Thomsen, H. T. Grahn, H. J. Maris, and J. Tauc. Surface generation and detection of phonons by picosecond light pulses. *Physical Review B*, 34(6):4129–4138, September 1986.
- [51] Alejandro Fainstein and Bernard Jusserand. Raman scattering in resonant cavities. In Manuel Cardona and Roberto Merlin, editors, *Light Scattering in Solid IX*, pages 17–110. Springer Berlin Heidelberg, Berlin, Heidelberg, 2007.
- [52] N. D. Lanzillotti-Kimura, A. Fainstein, B. Perrin, and B. Jusserand. Theory of coherent generation and detection of THz acoustic phonons using optical microcavities. *Physical Review B*, 84(6):064307, August 2011.
- [53] N. D. Lanzillotti-Kimura, A. Fainstein, A. Lemaitre, B. Jusserand, and B. Perrin. Coherent control of sub-terahertz confined acoustic nanowaves: Theory and experiments. *Physical Review B*, 84(11):115453, September 2011.
- [54] Tsun Hang Fung, Tom Veeken, David Payne, Binesh Veetil, Albert Polman, and Malcolm Abbott. Application and validity of the effective medium approximation to the optical properties of nano-textured silicon coated with a dielectric layer. *Optics Express*, 27(26):38645, December 2019.

- [55] Sanjay Gopal Ullattil and Pradeepan Periyat. Sol-Gel Synthesis of Titanium Dioxide. In Suresh C. Pillai and Sarah Hehir, editors, *Sol-Gel Materials for Energy, Environment and Electronic Applications*, pages 271–283. Springer International Publishing, Cham, 2017.
- [56] Li-Lan Yang, Yi-Sheng Lai, J.S. Chen, P.H. Tsai, C.L. Chen, and C. Jason Chang. Compositional Tailored Sol-Gel SiO_2 – TiO_2 Thin Films: Crystallization, Chemical Bonding Configuration, and Optical Properties. *Journal of Materials Research*, 20(11):3141–3149, November 2005.
- [57] C. R. Ottermann, R. Kuschnerit, O. Anderson, P. Hess, and K. Bange. Young’s Modulus and Density of thin TiO_2 Films Produced by Different Methods. *MRS Proceedings*, 436:251, 1996.
- [58] M C Ferrara, L Pilloni, S Mazzarelli, and L Tapfer. Hydrophilic and optical properties of nanostructured titania prepared by sol–gel dip coating. *Journal of Physics D: Applied Physics*, 43(9):095301, March 2010.
- [59] A.O Olofinjana, J.M Bell, and A.K Jämting. Evaluation of the mechanical properties of sol–gel-deposited titania films using ultra-micro-indentation method. *Wear*, 241(2):174–179, July 2000.
- [60] A Bendavid, P J Martin, and H Takikawa. Deposition and modification of titanium dioxide thin films by filtered arc deposition. *Thin Solid Films*, page 9, 2000.
- [61] Paulo Soares, Alexandre Mikowski, Carlos M. Lepienski, Emanuel Santos, Glória A. Soares, Vitoldo Swinka Filho, and Neide K. Kuromoto. Hardness and elastic modulus of TiO_2 anodic films measured by instrumented indentation. *Journal of Biomedical Materials Research Part B: Applied Biomaterials*, 84B(2):524–530, February 2008.
- [62] L. Borgese, M. Gelfi, E. Bontempi, P. Goudeau, G. Geandier, D. Thiaudière, and L.E. Depero. Young modulus and Poisson ratio measurements of TiO_2 thin films deposited with Atomic Layer Deposition. *Surface and Coatings Technology*, 206(8-9):2459–2463, January 2012.
- [63] O. Ortíz, M. Esmann, and N. D. Lanzillotti-Kimura. Phonon engineering with superlattices: Generalized nanomechanical potentials. *Physical Review B*, 100(8):085430, August 2019.
- [64] Diego F. Lionello, Juan Ignacio Ramallo, Galo J. A. A. Soler-Illia, and María Cecilia Fuertes. Mechanical properties of ordered mesoporous oxides thin films. *Journal of Sol-Gel Science and Technology*, 101(1):114–139, January 2022.
- [65] Diego F. Lionello, Paula Y. Steinberg, M. Mercedes Zalduendo, Galo J. A. A. Soler-Illia, Paula C. Angelomé, and M. Cecilia Fuertes. Structural and Mechanical Evolution of Mesoporous Films with Thermal Treatment: The Case of Brij 58 Templated Titania. *The Journal of Physical Chemistry C*, 121(40):22576–22586, October 2017.